Int. J. Heat Mass Transfer. Vol. 19, pp. 1197–1204. Pergamon Press 1976. Printed in Great Britain

TURBULENT BUOYANT JETS IN UNSTRATIFIED SURROUNDINGS

R. A. SEBAN* and M. M. BEHNIA†

(*Received* 15 *March* 1976)

Abstract—Comparison of the numerical and integral method solutions for the buoyant turbulent jet discharging vertically into unstratified surroundings of the same fluid show that essentially similar results are obtained when the property variation is small and appropriate turbulence parameters are used in the two kinds of calculation. Experimental results for a jet of heated air indicate correspondence with the predictions which, for the integral method, involve the entrainment coefficient appropriate to the isothermal jet. For specification of the entrainment coefficient for buoyancy, and a ratio of thermal to hydrodynamic widths which approaches unity as the flow approaches the asymptotic situation of the plume from a point source.

NOMENCLATURE

- b_u, b_T, width parameters for specification of Gaussian profiles for velocity and temperature;
- c, specific heat;
- g, gravitational acceleration;
- G, group $\dfrac{g\beta(T_c - T_\infty)r}{u_c^2}$, reciprocal of the square of a Froude number;
- l, mixing length;
- Q, total thermal energy in the flow;
- r, radial distance from centerline;
- T, absolute temperature;
- v, radial velocity;
- u, axial velocity;
- x, distance in the flow direction.

Greek symbols

- ν, kinematic viscosity;
- ρ, density;
- λ, ratio b_T/b_u in the region of developed flow.

Subscripts

- c, centerline;
- ∞, ambient;
- 0, at the nozzle outlet ($x = 0$);
- e, at the end of the region of flow development;
- m, mean value (mixed mean for temperature).

INTRODUCTION

THE SPECIFICATION of the temperature and velocity profiles in an upward directed, turbulent, buoyant jet in unstratified surroundings is not yet fully established because of ambiguities related to the region of flow development and to some continuing uncertainty about the parameters that are needed to characterize the turbulent flow in the region in which the flow is fully developed. Here the numerical and integral methods of prediction of the flow are reviewed and the predictions thereof are compared on the basis of the parameters which best relate these predictions to experimental results for the temperature and velocity fields that have been obtained for the vertical discharge of heated air through a round jet into ambient, unstratified, air surroundings.

NUMERICAL METHOD

Given the initial velocity and temperature profiles issuing from the jet, the boundary layer forms of the momentum and energy equations can be solved numerically by the method of Patankar and Spalding [1]. If these initial profiles are taken to be uniform, economy in the incrementing of the lateral domain is achieved by concentrating the calculation in the shear layer that develops initially, with the uniform velocity in the interior of this shear layer varying as $u(\mathrm{d}u/\mathrm{d}x) = g[(\rho_\infty/\rho) - 1]$. Even with this arrangement, exceedingly small forward steps are required initially where the flow is laminar and this restraint can be relieved at first defining entrainment on the inner and outer edges of the shear layer from Lock's [2] analytical solution for the development of the shear layer between parallel streams.

A position of transition to turbulence must be selected and the choice is uncertain in terms of available results. Liepmann and Laufer [3] specified transition at $u_0 x/\nu = 50\,000$ for an essentially two dimensional mixing zone, but many experiments on jets have inferred much smaller values of this Reynolds number. Cederwall [4] indicated that the flow from a jet appeared to be turbulent from the jet exit onward when the Reynolds number $u_0 r_0/\nu$ exceeded 1000, and for this value, transition at $x/r_0 = 1$ gives $u_0 x/\nu = 1000$. Clearly, the selection of the transition point is somewhat arbitrary.

After transition the single equation model of turbulence is used, as described by Launder [5], with the initial distribution of turbulent kinetic energy obtained

*Department of Mechanical Engineering, University of California at Berkeley.
†Research Assistant.

by equating the terms for the production and dissipation of kinetic energy and using the upstream, laminar, velocity profile in this evaluation. With this specification and the definition of the parameters of the turbulent flow model the turbulent flow calculation can proceed. When the inner surface of the shear layer meets the centerline, at $x = x_e$, the inner boundary condition becomes one of symmetry and the lateral incrementing of the flow thereafter extends from $0 < r < r_e$. In the present context the flow is considered to be "developed" after this location.

The turbulence model used here involved the factor of 0.50 in the term for the production of kinetic energy, and the factor 0.125 in the term for its dissipation. Turbulent Prandtl numbers were taken as 0.70 for thermal energy and 1.7 for kinetic energy. The mixing length was based on the distance Δr_l between the points at which the velocity ratios u/u_c were 0.99 and 0.10, the first ratio being taken different than unity to provide for a reasonable specification of Δr_l in the shear layer in the developing region. A linear augmentation of the mixing length due to relative buoyancy was included, and the mixing length was defined as

$$l = 0.1\Delta r_l\left[1 + B\frac{g\beta(T_c - T_\infty)}{u_c^2}\Delta r_l\right] \tag{1}$$

where for a gas β is taken as $1/T_\infty$.

With B taken as 14.1 this model gives results which coincide acceptably with the existing predictions for a plume above a point source and a jet issuing from a point source, and the use of the relative buoyancy factor in equation (1) eliminates the necessity of changing the ratio of $l/\Delta r_l$ for these two kinds of flow. The factor of course, is expressible in terms of the Richardson number as done by Koosinlin and Launder [6] and if that number is evaluated on the basis of Gaussian velocity and temperature profiles, with Δr_l as defined above, the value of $B = 14.3$ corresponds to a factor of 4.23 in the Koosinlin relation, where he used 5.0.

INTEGRAL METHOD

If density variation is accounted for only in the buoyant force term, then integration of the boundary layer forms of the continuity, momentum, and energy equation, gives, for constant density (unstratified) surroundings:

$$\frac{d}{dx}\int_0 ur\,dr = -(vr)_\infty \tag{2}$$

$$\frac{d}{dx}\int_0^\infty u^2 r\,dr = g\int_0^x \beta(T - T_\infty)r\,dr \tag{3}$$

$$\frac{d}{dx}\int_0^\infty u(T - T_\infty)r\,dr = 0. \tag{4}$$

If a Gaussian distribution is used for the profiles of the shear layer, so that $u/u_c = 1$, $r < r_u$; $u/u_c = e^{-[(r-r_u)/b_u]^2}$; $r > r_u$ and $(T - T_\infty)/(T_c - T_\infty) = 1$, $r < r_T$; $(T - T_x)/(T_c - T_x) = e^{-[(r-r_T)/b_T]^2}$, $r > r_T$; the integrals of equations (2)–(4) are specified in terms of b_u, b_T, r_u and r_T, the latter two of course defining the inner limits of velocity and temperature variation. Abraham [7] solved equations (3) and (4) in this way, choosing $r_u = r_T$ proportional to x, $b_T = 1.13b_u$ and $b_u/x = 0.13$, and as a consequence there were determined the distance x, at which $r_u = r_T = 0$, and u_c/u_0 at that location. Hirst [8] subsequently eliminated the assumption of r_u proportional to x and instead included equation (2), for which he defined an entrainment $-(vr)_\infty$ based on Albertson's [9] formulation for the non-buoyant situation, multiplied by a linear function of the buoyancy parameter evaluated at the jet outlet $[g\beta r_0(T - T_\infty)/u_0^2]$ the constant in this linear relationship being determined by comparison with Abraham's solution for small values of this parameter. In the present instance Abraham's solution was used for the developing region, but in a slightly altered form, based on the integration of equations (2) and (3) using average values for the integrals on the right, and the assumption of potential flow in the central region of the flow. Such an operation produces values of x_e/r_0, and b_u/r_0 and u_c/u_0 at the end of the development region, where the complete profile is first Gaussian, in terms of an average of an entrainment coefficient defined locally as $(-vr)_x = \alpha u_c b'$ where b' is the radius at which $u/u_c = 1/e$. This result was compared to that of Abraham and relatively good correspondence was obtained for an average α of $0.0424 + 0.2[g\beta(T - T_\infty)r_0/u_0^2]$. Figure 1 contains curves showing these results, and this figure contains a dashed curve to indicate Abraham's results for x_e/r_0. When b_u/r_0 and u_c/u_0 are known, equation (3) gives

$$b_T = \frac{b_u}{\left[\frac{u_c}{u_0}\left(\frac{b_u}{r_0}\right)^2 - 1\right]^{\frac{1}{2}}}. \tag{5}$$

This differs from Abraham's result in producing $b_T/b_u < 1$ at the beginning of the development region, because with buoyancy $u_c/u_0 > 1$ there.

Figure 1 contains points to indicate the results from the numerical calculation, made as indicated already, but with $B = 43$, the larger value being needed to obtain the correspondence of x_e/r_0 with Abraham's result. These calculations were made with relatively small values of $(T_0 - T_\infty)$, large values of the buoyancy being obtained by increasing g. Relatively large values of the jet Reynolds number, $u_0 r_0/\nu$ of the order of 2500 were used and transition was taken close to the nozzle, $(x/r_0) \approx 0.5$. The Reynolds number was large enough to essentially eliminate the effect of molecular transport as soon as the flow was made turbulent.

After the attainment of Gaussian profiles with r_T and r_u equal to zero, equations (2)–(4) take the familiar forms associated with the fully developed region, for which λ is defined as b_T/b_u:

$$\frac{d}{dx}u_c b_u^2 = 2\alpha u_c b_u \tag{2a}$$

$$\frac{d}{dx}u_c^2 b_u^2 = 2b_u^2 g\beta(T_c - T_\infty)\lambda^2 \tag{3a}$$

$$[u_c b_u^2(T_c - T_\infty)g\beta] = \frac{2}{\pi}\frac{Qg\beta}{\rho c}\frac{1 + \lambda^2}{\lambda^2}. \tag{4a}$$

Fox [10] integrated the equation for the kinetic

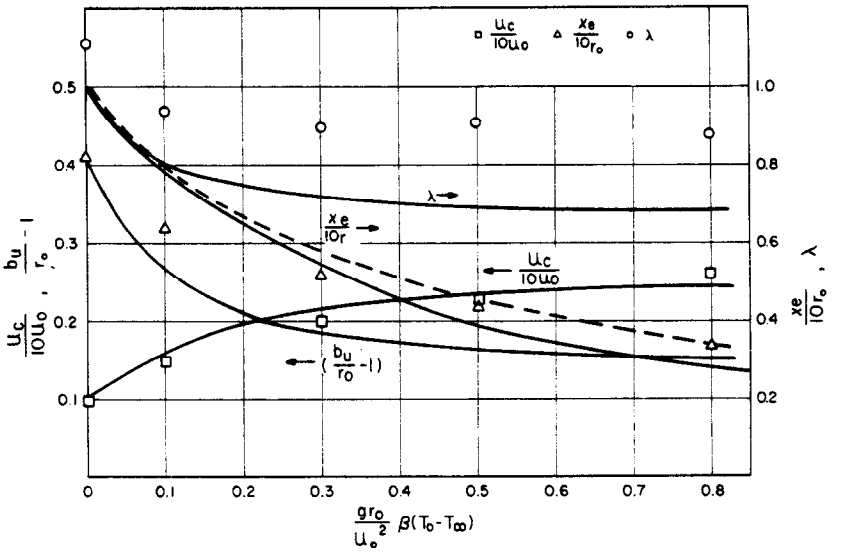

FIG. 1. Quantities at the end of the development region. The solid curves are the present interpretation based on Abraham's results: the dashed curve is Abraham's result for x_e/r_0. The points are the results from the numerical computation.

energy of the mean flow that is obtained by multiplying the momentum equation by u and by comparison of this integral form to the above forms of the continuity and momentum equation showed that the entrainment coefficient should be of the form

$$\alpha = \alpha_1 + \left(2 - \frac{3}{1+\lambda^2}\right)\lambda^2\left(\frac{b_u g\beta(T_c - T_\infty)}{u_c^2}\right).$$

It is implied but not necessary that α_1 be independent of the buoyancy; taken so, α_1 is then the entrainment coefficient of the non buoyant jet, for which a value of 0.055 is suitable and which was used herein. For plumes above a point source, for which λ is specified, equations (2a), (3a), (4a) can be integrated to give the usual power law forms $u_c \sim x^{-1/3}$, $(T_c - T_\infty) \sim x^{-5/3}$. Rouse and Yi [11] were among the first to do so for $\lambda = 1$. These equations can also be integrated analytically from initial conditions such as defined on Fig. 1 but only for $\lambda = 1$. But this value of λ is inconsistent, since to satisfy the energy equation, equation (5), λ must be less than unity at that location.

To allow for a variation of λ from its initial value, another relation can be obtained from the energy equation multiplied by $(T - T_\infty)$ and then integrated. This is like Fox's procedure, except that this new equation has no physical significance. The ultimate result is the equation

$$\frac{d}{dx}\left[\left(\frac{\lambda^2}{\lambda^2+2}\right)(b_u^2 u_c)(T_c - T_\infty)^2 (g\beta)^2\right] = -\frac{2}{3}\frac{\alpha_1}{\sigma_t} u_c b_u (g\beta)^2 (T_c - T_\infty)^2. \quad (6)$$

Here σ_t is the turbulent Prandtl number; when it is specified, equation (5) determines λ. For the plume and for the non buoyant jet originating from point sources, equation (6) does indicate a constant value of λ, depending upon the turbulent Prandtl number. For the plume $\sigma_t = 0.60$ gives $\lambda = 1$.

For the jet, $G_0 = 0$, the integral solution is asymptotic to the solution for a jet issuing from a point source, and the choice of $\sigma_t = 0.60$ in the integral solution yields $\lambda = 1.55$. The numerical solution gives a final λ of 1.20 and is indicated on Fig. 4 to approach the asymptote for this value of λ. The latter is preferable in terms of available results, though the present measurements of centerline temperature appear to be in better accord with the former.

SOLUTION

Figure 2 shows the centerline temperatures that are predicted by the numerical and the integral methods

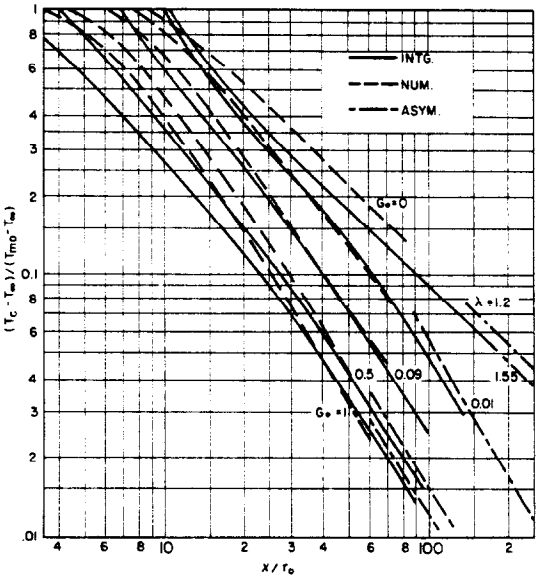

FIG. 2. The centerline temperature. Solid curves are predictions from the integral solution, dashed curves give the predictions from the numerical calculations and also the plume asymptotes. Asymptotes are given both for $\lambda = 1.2$ and 1.55 for the jet, $G_0 = 0$.

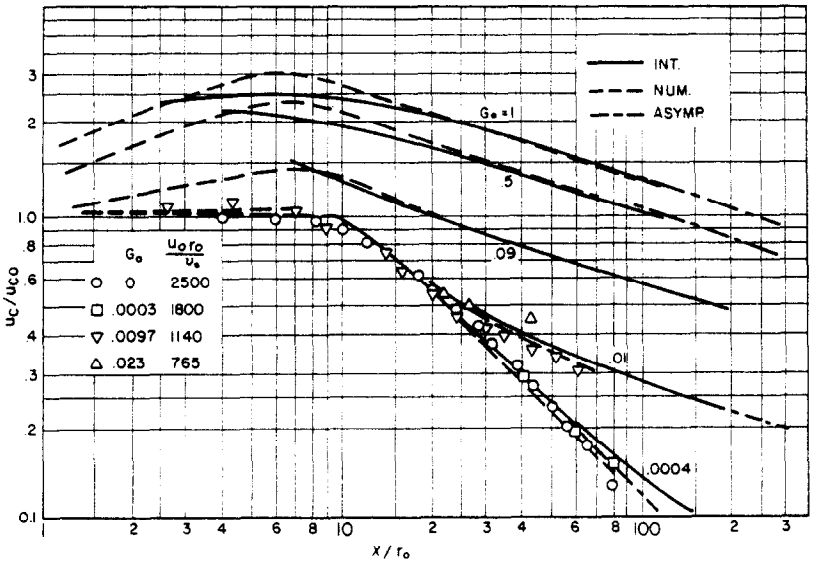

FIG. 3. The centerline velocity.

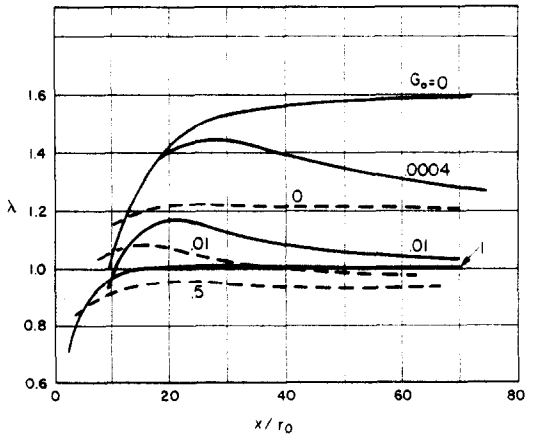

FIG. 4. Ratio of thermal and velocity widths. Solid curves are from the integral solution; dashed curves are from the numerical solution. The curves begin at $x = x_e$; Fig. 1.

of solution, with dashed curves used for the numerical and solid curves for the integral results. These begin at slightly different values of x_e/r_0, as indicated by the differences in the integral and numerical results on Fig. 1. For buoyant jets, on the figure

$$G_0 = \frac{g\beta(T_0 - T_\infty)r_0}{u_0^2}.$$

These results soon converge and ultimately approach the asymptotes that are indicated on the figure, which are the predictions for the plume above a point source, with $\alpha_1 = 0.055$, $\lambda = 1$, and Fox's specification of α, giving $\alpha = 0.092$. There is a difference for the jet, $G_0 = 0$. For this case the numerical and integral solutions are not the same and each tends to its individual asymptote, for $\lambda = 1.2$ and $\lambda = 1.55$ as already noted.

Figure 3 shows the centerline velocities, for which there is general accord for the two methods of prediction. There the solid curves, from the integral method, begin with the values indicated for the starting point as given by Fig. 1.

Figure 4 shows the values of λ associated with the two kinds of solution. For the solid curves associated with the results from the integral method, the asymptote is 1.55 for $G_0 = 0$ and 1.0 for $G_0 > 0$. For $G_0 > 0$ the numerical method was not run far enough to determine the asymptote, but it appears to be about $\lambda = 0.95$. In this respect it is to be noted that the radial velocity and temperature profiles are not quite Gaussian, being slightly lower for $r/b < 1$ and slightly higher for $r/b > 1$. Thus, the comparison that is made for λ, with b evaluated at $1/e$ of the centerline value, with the λ of the Gaussian profiles is not a very direct approach. The profile shapes given by the numerical method are, in fact, closer to those predicted by Schmidt [12], but the profiles of the numerical solution are also not quite similar in respect to the distance, x.

EXPERIMENTS

Temperature and velocity measurements, by means of a thermocouple and hot film anemometer, were made in a heated air jet directed vertically upward at the center of a rectangular enclosure 1.4 × 1.4 m in plan and 1.7 m high from a 10 cm high screened opening at the floor to a 5 cm high screened opening at the top, above which a top enclosure extended another 0.64 m. Numerous thermocouples were located in one corner and at the center of an opposite side of the enclosure for the measurement of ambient air temperature, which for the data cited here was invariable with height.

The jet was produced by nozzles with $r_0 = 1.15$ and 0.5 cm and these were mounted on a tube with an inside radius of 1.15 cm. At 7.1 cm below the nozzle mounting flange there was a mitre turn to the horizontal. The horizontal portion of the tube contained an electrical cartridge heater, with the supply air passing through the 1.2 mm annular space between the tube and the outside of the heater. The space between the end of the heater and the bottom of the nozzle was filled with

stainless steel wool to aid in the equalization of velocity and temperature. Particularly with the larger nozzle, for which there was no contraction from the plenum, this produced somewhat irregular velocity profiles, which were but marginally improved by the addition of hardware cloth screen between the nozzle and the plenum. With the contraction produced by the smaller nozzle, the velocity profile was uniform at the outlet, except near the outer radius, though because of the smaller size the ratio of mean to centerline velocity for the small nozzle 0.82, was less than the 0.91 of the larger nozzle. Temperatures were relatively uniform over the central region of the flow, but showed a substantial drop near the wall of the nozzle, to the extent that the central temperature exceeded substantially the mean value as the magnitude of the temperature was increased.

Because of the low efficiency involved in the heating of the air the losses were substantial, and the plenum-heater assembly was water jacketed outside of its insulation to avoid the production of a plume by the losses from that unit.

The air was metered before introduction to the heater, and the relative radial distribution of velocity at the nozzle outlet was determined with the hot film when operating with air at room temperature. The mass balance then gave absolute values and thus the absolute hot film calibration for low temperatures, with the film at the nozzle center. At elevated temperatures it was assumed that the velocity profile, u/u_m, remained the same as it was at low temperatures and then a radial temperature distribution measurement specified the absolute velocities and the total energy rate. The high temperature film calibration was based on the velocity calculated this way.

Since the buoyancy factor, evaluated as

$$G_0 = \frac{g\beta(T_{m0} - T_\infty)r_0}{u_{m0}^2}$$

depends on the cube of the nozzle radius for a given mass flow rate, high values of the buoyancy could only be obtained with the larger nozzle by the use of values of $(T_{m0} - T_\infty)$ as large as 160°C, and with low mass flows, so that the nozzle Reynolds numbers became as low as 177. This restricted the appraisal of the flow development region, as is indicated in the results that follow.

The temperatures and velocities that are shown as the results are mean values obtained by averaging with respect to time, for periods of about a minute, the fluctuating signal as recorded on a strip chart. This fluctuation, of relatively long period (of the order of 5 s), was greatest in the region of x/r 20, where for temperature the ratio of the amplitude to the mean value of $(T - T_\infty)$ was almost 0.30; this decreased to 0.085 at $x/r_0 = 57$. The effect increases with the amount of buoyancy. Radially it is highest away from the centerline and remains significant to the outer edge of the flow.

As noted, all the results presented here were obtained with the top on the enclosure, so that communication with the exterior was only through the two screened openings. Despite the relatively small size of the flow relative to that of the enclosure, the enclosure had some effect, as could be discerned when the top section was removed. There was no effect for $G_0 = 0$ but effects were discernible for G_0 as low as 0.01; there the centerline temperatures were relatively lower, corresponding asymptotically to a value of $\alpha = 0.11$ rather than 0.092, with a corresponding increase in width of the flow. The operation with the top on the enclosure was chosen as desirable to avoid jet fluctuations, and causing no more boundary constraint than in most comparable experiments, but the sensitivity of the entrainment to the nature of the enclosure has not yet been explained.

CENTERLINE TEMPERATURES

Figure 5 contains some of the curves for the integral solution that were shown in Fig. 1, and also contains centerline temperatures, T_c, evaluated as $(T_c - T_\infty)/(T_{m0} - T_\infty)$, where T_{m0} is the mixed mean exit temperature, that data being shown only for the whole region of developed flow and there only for low values of G_0.

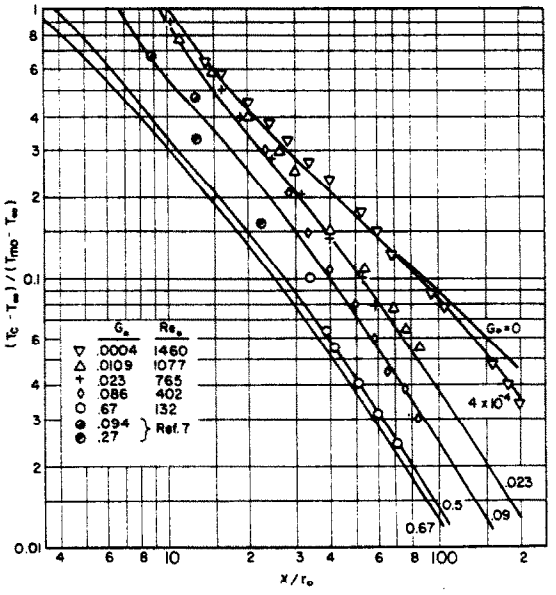

FIG. 5. Experimental values of the centerline temperature. Solid curves are from the integral solution, as on Fig. 2. The results of Abraham [7] are for a Reynolds number over 1300.

For the data, G_0 was evaluated with β taken as $1/T_\infty$. Because T_{c0}, the temperature at the jet centerline, exceeded T_{m0} more severely as G_0 increased, the ratio $(T_{c0} - T_\infty)/(T_{m0} - T_\infty)$ being as much as 1.6 for $G_0 = 0.67$, the ratio $(T_c - T_\infty)/(T_{m0} - T_\infty)$ in the development zone exceeds unity, sometimes substantially. As is shown elsewhere [15] the value of $(T_c - T_\infty)/(T_{m0} - T_\infty)$ begins to drop below unity near $x/r_0 = 4$, and attains a value near 0.90 at $x/r = 8$ for $G \to 0$ and at about $x/r_0 = 6$ for $G_0 = 0.26$. This is at least the trend indicated by the theory as shown on Fig. 2 but the results scatter and are thus not conclusive enough for a direct appraisal of the theory, particularly as the effect of transition length is also involved. Later, more consideration is given to the effect of low nozzle Reynolds

numbers but the representation of Fig. 5 contains data only for relatively long values of the x/r_0 where that data approaches the theoretical values from above. A separate analysis by the integral method accounted for $(T_{c0}-T_\infty)>(T_{m0}-T_\infty)$ by an adjustment of the value of λ given by equation (5) at $x=x_e$ to accommodate this excess and this revealed a very rapid change in λ in the region immediately downstream of $x=x_e$ so that $(T_c-T_m)/(T_{m0}-T_\infty)$ attained practically the same value for $1<(T_{c0}-T_\infty)/(T_{m0}-T_\infty)<1.6$ as it did for $(T_{c0}-T_\infty)=(T_{m0}-T_\infty)$ after the former ratio (the ordinate of Fig. 5) was less than 0.85.

The results that are shown on Fig. 5 show that the integral method predicts adequately the experimental centerline temperature for all $x>x_e$ when x_e as predicted is approximately correct and for $x\gg x_e$, but less than that needed for asymptotic behavior, when the results exceed the prediction in $x>x_e$.

Figure 5 also contains four points due to Abraham, obtained with Reynolds numbers above 1300 using salt solutions in water to produce buoyancy, which tend to confirm better the predictions in the region of x near x_e and support his appraisals of the length of the development region.

CENTERLINE VELOCITIES

Figure 3 contains experimental centerline velocities for low values of G_0, most of which were obtained with a hot film anemometer using the calibration as already described, but some of which were obtained with a hot wire for which the calibration was calculated from geometry and the usual Nusselt number relation. The results from the former were apparently better near the nozzle, where the temperatures were high, and the latter far from the nozzle, where they were low. The data shown on Fig. 3 tend to confirm the predictions for the jet, $G_0=0$, and at least show the trends that are indicated by the theory for the values of G_0 that are greater than zero.

RADIAL VELOCITIES, TEMPERATURES AND WIDTHS

Radial velocity and temperature profiles were obtained at a number of locations but these are not shown here. In the region of developed flow these indicated profiles of the Gaussian type, though the data scatter was such that no further distinction about profile shape was possible. The measurement at $r>0$ involves greater amplitudes in the temporal variation already noted, with increased difficulty in averaging, and the accounts for some of the additional uncertainty in the radial profiles.

The top part of Fig. 6 shows the widths predicted for the jet, indicating the difference in $\lambda=b_r/b_u$ already shown on Fig. 4. Data are shown, being the radii for the occurrence of $1/e$ of the centerline value. The velocity width, which is about the same for both predictions, is relatively confirmed, but the thermal width, b_T, gives no definitive appraisal.

The lower part of Fig. 6 shows widths associated with two values of G_0, and the prediction for $G=0.1$. With this much buoyancy, λ is near unity for both the

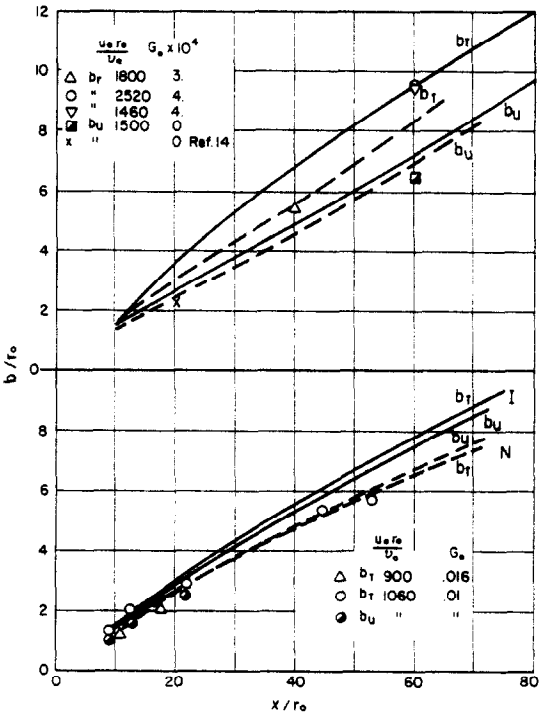

FIG. 6. Velocity and temperature widths. Solid curves are from the integral method, dashed curves from the numerical method.

integral and the numerical predictions. The data do indicate this, and for $x/r<25$ the predictions are so close together that the data cannot be used to indicate a preference. For larger x/r_0, for which only thermal widths are available, these are closer to the numerical prediction.

CENTERLINE TEMPERATURE AND VELOCITY WITH LOW REYNOLDS NUMBERS

The experimental values of the centerline temperature were not shown on Fig. 5 for large G_0 and small x/r_0 because they were substantially above the theory. It was indicated in the discussion relative to that figure that this discrepancy was probably not due to the fact that $(T_{c0}-T_\infty)>(T_{m0}-T_\infty)$ for these conditions and the difference was probably due to values of x_e larger than those predicted by Fig. 1 because of the low Reynolds numbers associated with the large values of G_0. Figure 7 shows the centerline temperatures for a Reynolds number of 177, with $G_0=0.26$, as $(T_c-T_\infty)/(T_{c0}-T_\infty)$. Curve B of that figure is the prediction for $G_0=0.25$, by the integral method, beginning with Fig. 1, shown for the region for which it would be reasonably valid for the ordinate used on Fig. 7, for the value of $(T_{c0}-T_\infty)=1.6\,(T_{m0}-T_\infty)$ that prevailed for these results. Curve A, as a contrast, is the integral prediction based on an arbitrary choice of $x_e/r_0=14.8$, with the associated starting values for the developing region obtained from Fig. 1 for this value of x_e/r_0, and λ further adjusted for the excess of centerline over the mean temperature at the nozzle. Once the calculation for developed flow is initiated, there is a precipitous drop in the predicted value of centerline temperature;

equation (5) rapidly increases the initially small λ to a value of the outer of unity. The data are near this prediction but they exhibit a different trend; they do confirm the prediction at large x/r_0, where the effect of the starting condition is no longer very important.

Curves C and D are the results of numerical calculation made with $u_{m0}r_0/\nu_0 = 177$ and the actual initial temperatures and velocities and transition lengths of x/r_0 of 13 and 10.4 respectively. In these numerical calculations the initial flow subdivision was taken in $0 < r < r_0$, so that an initial temperature profile could be taken to resemble that of the experiment, but this subdivision diminished the accuracy of shear layer development, since the incrementing was excessively large in the initial portion of this region. Thus, the

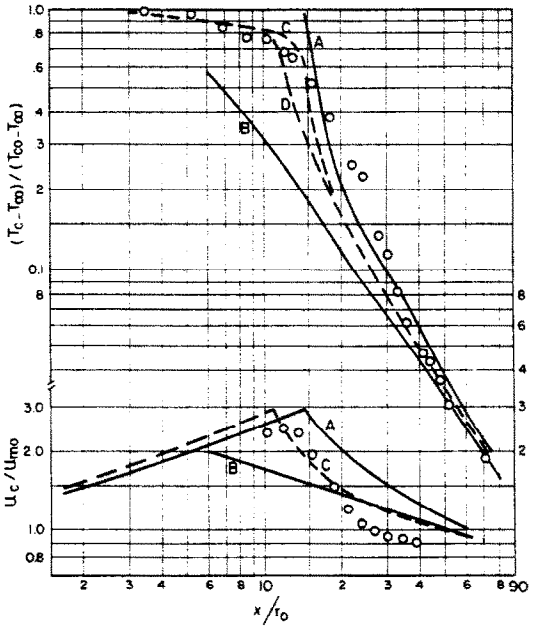

FIG. 7. Centerline temperature and velocity at low Reynolds number. The data are for $U_0r_0/\nu_0 = 177$, $G_0 = 0.26$; the predictions are for $G_0 = 0.25$. Curve A is the integral solution for $x_e = 14.8\ r_0$, and associated starting quantities from Fig. 1. Curve B is from Figs. 2 and 3. Curves C and D, dashed, are numerical solutions with $x_e = 13\ r_0$ and $10.4\ r_0$.

hydrodynamics of this result are somewhat questionable, but the full radial incrementing allows the centerline temperature to decrease because of molecular transport in the laminar flow region. Once transition occurs, the large eddy diffusivity that exists, due at least in part to the method of initiation of the value of the turbulent kinetic energy, produces a drop in temperature almost as great as produced by Curve A. The indication of the data is of a more gradual increase of the eddy transport.

Figure 7 also shows predicted values of u_c/u_m, which here become substantial initially because of the large distances that exist before eddy transport is initiated. Data obtained with the hot film anemometer are shown, which at first tend to confirm Curve C but for $x/r_0 > 20$ are below Curve B, which here is indicative also of the asymptotic behavior expected at longer distances. For $x/r_0 > 20$ the velocities for this run were less than 0.40 m/s and there is evidence from other runs that the instrument read too low in this range of velocities.

CONCLUSION

The buoyant jet discharging upward into ambient, unstratified surroundings of the same fluid has been investigated by means of an integral method of solution using Gaussian profiles, initiated at the end of a flow development region which in nature was close to that specified by Abraham. These solutions are relatively close to numerical solutions which, compatibly with Abraham's integral solution, were made turbulent immediately downstream of the nozzle. At large distances from the nozzle both solutions are nearly identical and tend to become asymptotic, corresponding to $\alpha_1 = 0.055$ and Fox's definition of α, as used in the integral solution, and the value of λ equal to unity with which it terminates.

Experimental results for centerline temperature agree with these theories for a relative buoyancy G_0 that is less than 0.02, for which in these experiments the nozzle Reynolds number, u_0r_0/ν_0, was greater than 750. At larger buoyancies $G_0 > 0.02$, for which the Reynolds number was less, agreement is not obtained at small x/r_0, but it is at large values for which the specification of flow development length is less important.

Results for velocities, and velocity and thermal widths, reveal a greater scatter, but they do generally support the theory at least for the lower values of G_0, for which the Reynolds numbers were greater than 750.

Acknowledgement—This research was supported by the National Science Foundation as part of Grant GI-34932.

REFERENCES

1. S. V. Patankar and D. B. Spalding, *Heat and Mass Transfer in Boundary Layers*, 2nd edn. Intertext Books, London (1970).
2. R. C. Lock, The velocity distribution in the boundary layer between parallel streams. *Q. J. Mech. Appl. Math.* **4**, 42–63 (1951).
3. H. W. Liepmann and J. Laufer, Jr., Investigation of free turbulent mixing. Nat. Adv. Comm. for Aeronautics, Tech. Note No. 125.
4. K. Cederwall, The initial mixing on jet disposal into a recipient, Laboratory Investigations, Chalmers Univ. of Tech., Division of Hydraulics (1963).
5. B. E. Launder and D. B. Spalding, *Mathematical Models of Turbulence*. Academic Press, New York (1972).
6. M. L. Koosinlin, B. E. Launder and B. I. Sharma, Prediction of momentum, heat and mass transfer in swirling, turbulent boundary layers, *J. Heat Mass Transfer* **96C**, 204 (1974).
7. G. Abraham, Jet diffusion in a stagnant ambient fluid, Delft Hydraulics Laboratory, Pub. No. 29 (1963).
8. E. Hirst, Analysis of buoyant jets within the zone of flow establishment, Oak Ridge National Laboratory, Report ORNL-TM-3470 (1971).
9. M. L. Albertson, Y. E. Dai, R. A. Jensen and H. Rouse, Diffusion of submerged jets, *Trans. Am. Soc. Civ. Engrs* **115**, 639–697 (1950).
10. D. G. Fox, Forced plumes in a stratified fluid, *J. Geophys. Res.* **75**, 6818 (1970).
11. H. Rouse, C. Yih and H. Humphreys, Gravitational con-

vection from a boundary source. *Tellus* **4**, 201 (1952).
12. J. O. Hinze, *Turbulence*. McGraw-Hill, New York (1969).
13. W. Schmidt, Turbulente Ausbreitung eines Stromer Erhitzer Luft. *Z. Angew. Math. Mech.* **21**, 265, 271 (1941).
14. S. Sami, T. Carmody and H. Rouse. Jet diffusion with region of flow establishment. *J. Fluid Mech.* **27**(2), 231–252 (1967).
15. M. Behnia, Temperature and velocities in buoyant jets. Ph.D. Dissertation, University of California at Berkeley (1976).

JETS TURBULENTS SOUS L'INFLUENCE DE FORCES DE GRAVITE ET DANS UNE ATMOSPHERE NON STRATIFIEE

Résumé—La comparaison des solutions du problème du jet turbulent se développant verticalement dans une atmosphère non stratifiée du même fluide, solutions obtenues par voie numérique et par méthode intégrale montre que les résultats sont essentiellement similaires lorsque les variations de propriété sont faibles et que les paramètres caractéristiques appropriés de la turbulence sont utilisés dans les deux types de calcul. Les résultats expérimentaux relatifs à un jet d'air chaud sont en accord avec les prévisions qui, dans le cas de la méthode intégrale, font appel à un coefficient d'entrainement relatif au jet isotherme, à la définition selon Fox du coefficient d'entrainement en convection naturelle, et au rapport des épaisseurs thermiques et hydrodynamiques qui tend vers l'unité lorsque l'écoulement approche la configuration asymptotique d'un sillage au dessus d'une source ponctuelle.

TURBULENTE AUFTRIEBSSTRAHLEN IN NICHTGESCHICHTETER UMGEBUNG

Zusammenfassung—Für turbulente Auftriebsstrahlen, die vertikal in eine nichtgeschichtete Umgebung des gleichen Fluides aufsteigen, wird ein Vergleich der numerischen Lösung mit der Lösung nach der Integralmethode angestellt. Dabei ergeben sich im wesentlichen ähnliche Ergebnisse, solange die Aenderung in den Stoffwerten gering ist und geeignete Turbulenzparameter bei beiden Rechnungsverfahren verwendet werden. Versuchsergebnisse für einen Warmluftstrahl zeigen eine Übereinstimmung mit den berechneten Werten. Bei der Integral methode wird dabei der Entrainment-Koeffizient für den isothermen Strahl, die Fox-Spezifikation für den durch Auftrieb bedingten Entrainment-Koeffizienten und ein Verhältnis der thermischen zur hydrodynamischen Breite verwendet; letzteres geht gegen 1, wenn die Strömung sich dem asymptotischen Fall der von einer punktförmigen Quelle ausgehenden Auftriebsströmung nähert.

ВСПЛЫВАНИЕ ТУРБУЛЕНТНЫХ СТРУЙ В НЕСТРАТИФИЦИРОВАННЫХ СРЕДАХ

Аннотация — Сравнение решений, полученных с помощью численных и интегральных методов для турбулентной струи, истекающей вертикально в нестратифицированную окружающую среду той же жидкости, показывает, что получены в основном схожие результаты при незначительном изменении свойств. В обоих случаях используются соответствующие параметры турбулентности. Экспериментальные данные для струи нагретого воздуха согласуются с расчетными, полученными интегральным методом и с учетом коэффициента уноса, что соответствует случаю изотермической струи, конвективного коэффициента уноса по Фоксу, а также с учетом отношения тепловой ширины к гидродинамической, которое приближается к единице по мере того, как поток стремится к асимптотическому состоянию струи от точечного источника.